Chen, Min; Avarmaa, Katri; Taskinen, Pekka; Klemettinen, Lassi; Michallik, Radoslaw; O'Brien, Hugh; Jokilaakso, Ari

Handling trace elements in WEEE recycling through copper smelting-an experimental and thermodynamic study

Published in:
Minerals Engineering

DOI:
10.1016/j.mineng.2021.107189

Published: 01/11/2021

Document Version
Publisher's PDF, also known as Version of record

Please cite the original version:
Chen, M., Avarmaa, K., Taskinen, P., Klemettinen, L., Michallik, R., O'Brien, H., & Jokilaakso, A. (2021). Handling trace elements in WEEE recycling through copper smelting-an experimental and thermodynamic study. *Minerals Engineering*, *173*, Article 107189. https://doi.org/10.1016/j.mineng.2021.107189

Minerals Engineering 173 (2021) 107189

Contents lists available at ScienceDirect

Minerals Engineering

journal homepage: www.elsevier.com/locate/mineng

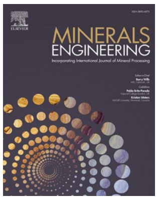

Handling trace elements in WEEE recycling through copper smelting-an experimental and thermodynamic study

Min Chen [a], Katri Avarmaa [a], Pekka Taskinen [a], Lassi Klemettinen [a], Radoslaw Michallik [b], Hugh O'Brien [b], Ari Jokilaakso [a,*]

[a] Department of Chemical and Metallurgical Engineering, School of Chemical Engineering, Aalto University, Kemistintie 1F, P.O. Box 16100, FI-00076 Aalto, Finland
[b] Geological Survey of Finland, Vuorimiehentie 2, 02150 Espoo, Finland

ARTICLE INFO

Keywords:
Trace elements
WEEE
Circular economy
Resource efficiency
Copper smelting

ABSTRACT

Recycling of waste electrical and electronic equipment (WEEE) is attracting increasing attention, due to the presence of valuable metals and the risk of environmental emissions associated with WEEE disposal. In this study, the distributions of trace elements (Ag, Ni, Co, and Sn) between copper alloy and magnetite/wüstite-saturated iron silicate slags were investigated at 1200–1300 °C and P_{O2} of 10^{-10}-$10^{-6.5}$ atm, simulating the conditions of WEEE reprocessing through secondary copper smelting and converting. The high-temperature isothermal equilibration experiments were conducted in synthesized magnetite/wüstite crucibles under controlled CO-CO_2 atmospheres followed by quenching in an ice-water mixture. The phase compositions and concentrations of the trace elements in copper alloy, magnetite/wüstite, and slag were determined by Electron Probe X-ray Microanalysis and Laser Ablation-High-Resolution Inductively Coupled Plasma-Mass Spectrometry. The distribution coefficients of all investigated trace elements between copper alloy and slag increased with decreasing oxygen partial pressure and increasing temperature. Ag distributed strongly into the copper alloy at all conditions, whereas Co mainly deported into the slag phase. Ni and Sn were concentrated in the alloy at lower P_{O2} and in the slag at higher P_{O2}. Varying concentrations of Ni, Co, and Sn were also dissolved into the solid magnetite/wüstite phase.

1. Introduction

The rapid development of the electronic information industry and the rapid upgrading of electronic devices have resulted in a surge of waste electrical and electronic equipment (WEEE) (Marinello and Gamberini, 2021). As the second largest WEEE generator after Asia, the production of WEEE in European Union is currently estimated to be approximately 11.6 million tonnes per year (Ibanescu et al., 2018). Motivated by stronger legislation, economic and environmental factors, efforts concerning recycling of WEEE are of high interest and in high demand (Directive, 2012; Messmann et al., 2019).

WEEE is a heterogeneous combination of metallic and non-metallic materials, including plastics, ceramics, copper, precious metals (Au, Ag, Pt, and Pd), heavy metals (Pb, Hg, Cr, and As, etc.) and other typical trace elements (Ni, Co, and Sn) (Zhang and Xu, 2016; Wang et al., 2017; Cesaro et al., 2018; Cui and Zhang, 2008; Zeng et al., 2018; Shuva et al., 2016), indicating WEEE can be an important raw material in many copper smelters (Lehner et al., 1999; Veldhuizen and Sippel, 1994; Hagelüken, 2006; Hagelüken and Corti, 2010; Lennartsson et al., 2018; Flores et al., 2014; Brusselaers et al., 2006; Khaliq et al., 2014) for recovering metal values. The route for WEEE recycling involves collection, dismantling, shredding and, crushing, followed by hydro-/pyrometallurgical processing. From the perspective of industrial practice, WEEE recycling, especially its copper-rich scrap fraction, is currently mainly performed through pyrometallurgical copper smelting routes (Tesfaye et al., 2017), due to the advantages of easy separation of precious metals from base metals, large capacity, high yields and convenient disposal of flue gas. Compared with available primary copper smelters, a wider variety of WEEE can be incorporated into the secondary copper smelters and subsequently produce copper as well as valuable side products of multiple precious and critical elements (Anindya et al., 2009). Among those secondary copper smelting routes, the processing of WEEE in TSL furnaces, like Ausmelt and Isasmelt technologies, are commonly used (Shuva et al., 2017). The precious and

---

* Corresponding author.
E-mail addresses: minchen0901@hotmail.com (M. Chen), katri.avarmaa@aalto.fi (K. Avarmaa), pekka.taskinen@aalto.fi (P. Taskinen), lassi.klemettinen@aalto.fi (L. Klemettinen), radoslaw.michallik@gtk.fi (R. Michallik), hugh.obrien@gtk.fi (H. O'Brien), ari.jokilaakso@aalto.fi (A. Jokilaakso).

https://doi.org/10.1016/j.mineng.2021.107189
Received 4 June 2021; Received in revised form 23 August 2021; Accepted 6 September 2021

trace elements are introduced into the TSL furnace along with secondary materials like WEEE and the metals distribute in smelting and converting into metal, slag, and gas phases. The subsequent converting and refining operations in the same furnace are energy-saving and effective recovery routes for extracting metal values from the valuable metals-enriched copper. Fig. 1 shows the route for WEEE recycling through secondary copper smelting.

There is a wealth of data revealing the distribution of Ag in pyrometallurgical copper smelting processes. A detailed literature review for the distribution of Ag can be found in our previous studies (Chen et al., 2020; Chen et al., 2021). Table 1 summarizes the details of the most recent experimental studies (Anindya et al., 2013; Avarmaa et al., 2018a, 2019, Dańczak et al., 2020, 2021; Derin and Yücel, 2002; Gortais et al., 1994; Kashima et al., 1978; Kho et al., 2006; Klemettinen et al., 2019; Nagamori and Mackey, 1977; Reddy and Healy, 1981a,b, Ren et al., 2020, 2021, Sukhomlinov et al., 2019a,b, 2020; Takeda et al., 1983; Tirronen et al., 2017; Wang et al., 1973; Klemettinen et al., 2018; Avarmaa and Taskinen, 2018b; Avarmaa et al., 2017; Sukhomlinov and Taskinen, 2017; Van den Bulck et al., 2018; Reddy, 1980; Louey and Swinbourne, & D.R., Lehner, T, 1999) for investigating the behavior of selected trace elements (Ni, Co, and Sn) in copper smelting processes. Apart from the above mentioned primary and secondary copper smelting routes, the distributions of trace elements in other pyrometallurgical processes and theoretical thermodynamic analyses have been reported by many researchers (Choi and Cho, 1997; Hellstén et al., 2019; Holland et al., 2019; Nakajima et al., 2011; Piskunen et al., 2018; Takeda et al., 1990; Teague et al., 2001; Wang et al., 1974; Xu et al., 2012, 2013; Yazawa, 1980; Nagamori and Mackey, 1978; Holland et al., 2018).

In those previous studies shown in Table 1, the behaviors of trace elements have been investigated extensively between metallic copper/sulfide copper matte and Al-Fe spinel/silica-saturated slags (Avarmaa et al., 2018a, 2019, Dańczak et al., 2020, 2021; Derin and Yücel, 2002; Kashima et al., 1978; Klemettinen et al., 2019; Nagamori and Mackey, 1977; Reddy and Healy, 1981a,b, Ren et al., 2020, 2021, Sukhomlinov et al., 2019a,b, 2020; Wang et al., 1973; Klemettinen et al., 2018; Avarmaa and Taskinen, 2018b; Avarmaa et al., 2017; Sukhomlinov and Taskinen, 2017; Van den Bulck et al., 2018; Reddy, 1980), but none at magnetite/wüstite saturation. Moreover, the chemical analysis methods used in some earlier studies (Ren et al., 2021; Ren et al., 2020; Kashima et al., 1978; Reddy and Healy, 1981; Reddy and Healy, 1981; Reddy, 1980; Anindya et al., 2013; Kho et al., 2006; Gortais et al., 1994; Takeda et al., 1983; Louey and Swinbourne, & D.R., Lehner, T. , 1999) may have caused inaccuracies when measuring the concentrations of trace elements in metal, matte, and slag, due to the incomplete phase separations. To overcome the difficulties of accurately determining the trace element concentrations in separate phases, direct phase microanalysis techniques were applied, thus avoiding distorted results caused by imperfect bulk sample separation.

This study aims to measure the distributions of Ag, Ni, Co, and Sn between copper alloy and magnetite/wüstite-saturated iron silicate slags, related to WEEE recycling in secondary copper smelting. The present results help to predict the conditions favorable for recycling valuable metals from WEEE into the copper alloy phase. The distributions of valuable metals between copper alloy and slag provide potential for improving recoveries of valuable metals from WEEE through adjusting the slag composition, temperature, and oxygen partial pressure. The trace element behaviors in the Cu-Fe-O-Si system have been investigated so far in slags at silica-saturation in previous studies (Sukhomlinov et al., 2019a,b; Sukhomlinov and Taskinen, 2017).

2. Experimental

High purity powders, shown in Table 2, were used for preparing the copper alloy and slag. The concentration of each trace element added into the copper alloy mixture was approximately 1 wt pct. The Fe_2O_3/SiO_2 ratio of initial slag mixture was determined based on the prediction of the FeO_x-SiO_2 phase diagram (Fig. 2) at copper saturation, simulated by MTDATA (Gisby et al., 2017; Davies et al., 2002) thermodynamic software using the MTOX database (Davies et al., 2002). Fig. 2 shows that the slag is saturated with wüstite (FeO) at 1200–1250 °C and $P_{O2} < 10^{-8}$ atm but is saturated with magnetite (Fe_3O_4) at higher P_{O2}. At 1300 °C, the slag is wüstite-saturated at P_{O2} of 10^{-8} atm but is magnetite-saturated at $P_{O2} = 10^{-7}$-10^{-6} atm.

Approximately 0.2 g of copper alloy mixture was equilibrated with equal amount of slag mixture in each experiment. The copper alloy mixture and slag mixture were loaded into a mold and then pressed into a pellet using a hydraulic press under high pressure of five tons. Magnetite (Fe_3O_4) and wüstite (FeO) crucibles were used for holding the sample pellet. The type of crucibles used at different conditions was determined based on the saturation of slags predicted by MTDATA. The magnetite and wüstite crucibles were prepared by oxidizing the iron foil at 1250 °C and P_{O2} of 10^{-7} and 10^{-10} atm, respectively. Before being oxidized, the iron foil was folded into a crucible shape and the bottom was formed into a bowl shape using a hemispherical stamping rod. The compositions of the crucibles were measured and validated by electron probe microanalysis. The atmosphere in the furnace was controlled by flowing CO-CO_2 gas mixtures. The gas flowrates calculated by HSC Chemistry software (Roine, 2017) for each target P_{O2} and the initial Fe_2O_3/SiO_2 ratios are listed in Table 3.

A vertical tube furnace (Nabertherm, Lilienthal, Germany, RHTV 120–150/1) equipped with $MoSi_2$ heating elements was used for conducting the high-temperature equilibration experiments. The

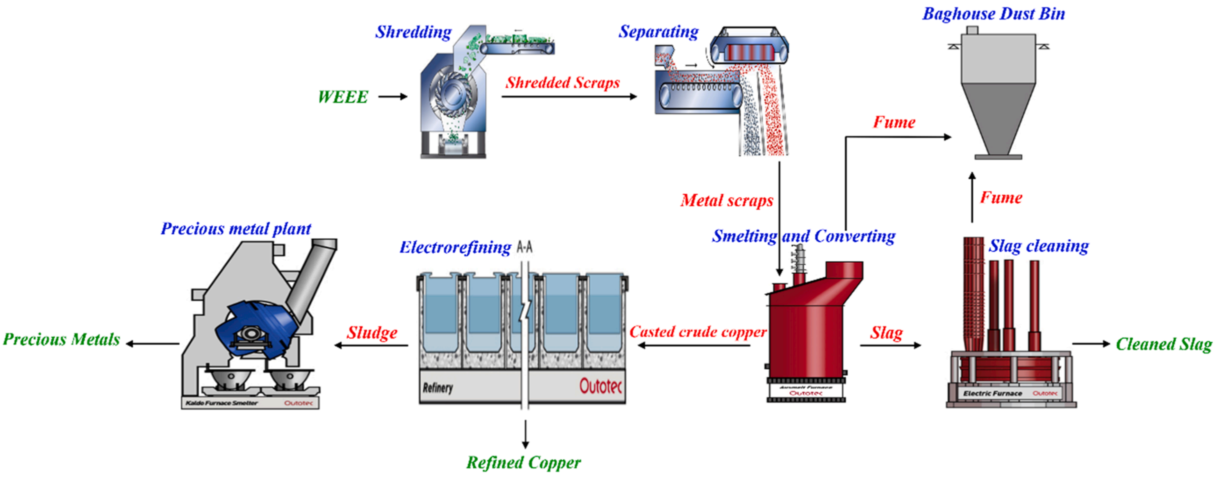

Fig. 1. The pyrometallurgical WEEE recycling route through secondary copper smelting.

Table 1
A summary table of most recent literature sources investigating the selected trace elements distributions in copper smelting.

Equilibrium System	Slag	LogP_{O2}/atm	T/°C	Elements	Crucible	Analytical methods	Ref.
Al_2O_3/(Al-Fe) Spinel saturated slag							
Copper alloy-slag	FeO_x-SiO_2-(K_2O)	−10 to −5	1300	Sn, Ni	Alumina	EPMA and LA-ICP-MS	(Klemettinen et al., 2019; Klemettinen et al., 2018)
Copper alloy-slag	FeO_x-SiO_2-Al_2O_3-(MgO)	−11 to −8	1300	Sn, Ni, Co	Alumina	EPMA and LA-ICP-MS	(Dańczak et al., 2020; Dańczak et al., 2021)
Copper alloy-slag	FeO_x-SiO_2-(Al_2O_3-CaO-K_2O)	−10 to −5	1300	Sn	Alumina	EPMA and LA-ICP-MS	(Avarmaa et al., 2018a, 2019)
Copper alloy-slag	FeO_x-SiO_2-Al_2O_3	−10 to −5	1300	Sn	Alumina	EPMA	(Avarmaa and Taskinen, 2018b; Avarmaa et al., 2017)
Copper alloy-slag	FeO_x-SiO_2-Al_2O_3-$CuO_{0.5}$	−11 to −6	1200–1300	Sn	Alumina	Polarographic techniques	(Nagamori and Mackey, 1977)
Copper alloy-slag	MnO-SiO_2-Al_2O_3	−12 to −10	1300–1350	Co	Alumina	AAS	(Ren et al., 2021)
Copper alloy-slag	FeO_x-SiO_2-Al_2O_3	−10 to −8	1400	Co	Alumina	Not reported	(Derin and Yücel, 2002)
SiO_2 saturated slag							
Copper alloy-slag	FeO_x-SiO_2-(Al_2O_3-CaO-K_2O)	−10 to −5	1300	Sn	Silica	EPMA and LA-HR ICP-MS	(Avarmaa et al., 2019)
Copper alloy-slag	FeO_x-SiO_2-Al_2O_3-(CaO)	−10 to −5	1300	Sn	Silica	EPMA	(Avarmaa and Taskinen, 2018b; Sukhomlinov et al., 2020)
Copper alloy-slag	FeO_x-SiO_2	−8 to −4	1250–1350	Ni, Co	Silica	EPMA and LA-ICP-MS	(Sukhomlinov et al., 2019a; Sukhomlinov and Taskinen, 2017)
Copper matte-slag	FeO_x-SiO_2-(Al_2O_3-CaO)	−8 to −7	1300	Sn	Silica	EPMA and LA-ICP-MS	(Sukhomlinov et al., 2019b)
Copper alloy-slag	MnO-SiO_2	−12 to −10	1350	Co	Silica	AAS	(Ren et al., 2020)
Copper alloy-white metal-slag	FeO_x-SiO_2	Not reported	1300	Ni, Co	Silica	AAS	(Kashima et al., 1978)
Copper alloy-slag	FeO_x-SiO_2-CaO-CuO_y	Not reported	1300	Sn	Silica	EPMA	(Van den Bulck et al., 2018)
Copper alloy-slag	FeO_x-SiO_2	−10 to −6	1250–1350	Co	Alumina	Gravimetric technique and XRF	(Wang et al., 1973)
Copper alloy-slag	Cu_2O-SiO_2	Not reported	1200–1250	Co	Silica	AAS, XRD, and SEM-EDS	(Reddy and Healy, 1981; Reddy and Healy, 1981; Reddy, 1980)
MgO saturated slag							
Copper alloy-slag	FeO_x-SiO_2-CaO	−7	1300	Sn	Magnesia	ICP-AES	(Anindya et al., 2013)
Copper matte-slag	FeO_x-SiO_2	Not reported	1250	Co	Magnesia	ICP-AES	(Kho et al., 2006)
Copper alloy-slag	CaF_2-CaO-MgO-SiO_2	Not reported	1227	Ni, Sn	Magnesia	ICP and XRF	(Gortais et al., 1994)
Copper alloy-slag	FeO_x-CaO	−12 to −5	1250	Sn, Ni, Co	Magnesia	AAS	(Takeda et al., 1983)
Copper matte-slag	FeO_x-SiO_2	Not reported	1250	Sn	Magnesia	ICP-AES	(Louey and Swinbourne, & D.R., Lehner, T. , 1999)
Magnetite saturated slag							
Copper alloy-copper matte-slag	FeO_x-SiO_2	Not reported	1200–1275	Ni, Co	Silica	EPMA and LA-ICP-MS	(Tirronen et al., 2017)

AAS: Atomic absorption spectroscopy.
XRF: X-ray fluorescence spectroscopy.
XRD: X-ray diffractometry.
ICP: Inductively coupled plasma spectroscopy.
ICP-AES: Inductively coupled plasma atomic emission spectrometry.
LA-ICP-MS: Laser Ablation Inductively Coupled Plasma-Mass Spectrometry.

Table 2
Materials used for preparing the copper alloy and slag.

Material	Quality/Purity	Supplier
Fe_2O_3	99.998 wt pct	Alfa Aesar
SiO_2	−40 mesh, 99.995 wt pct	Alfa Aesar
Cu	−625 mesh, 99.9 wt pct	Alfa Aesar
Ag	−100 mesh, 99.95 wt pct	Alfa Aesar
Ni	−120 mesh, 99.996 wt pct	Alfa Aesar
Co	−1.6 μm, 99.8 wt pct	Alfa Aesar
Sn	−100 mesh, 99.85 wt pct	Alfa Aesar
CO	99.99 vol pct	AGA-Linde (Finland)
CO_2	99.999 vol pct	AGA-Linde (Finland)
Iron foil	thickness 0.25 mm, 99.5 wt pct	Sigma Aldrich & Merck

temperature of the furnace was regulated by a Nabertherm P310 temperature controller. A calibrated S-type Pt/Pt-10 wt pct Rh thermocouple (Johnson-Matthey Noble Metals, UK), placed next to the sample, was used for measuring the furnace hot-zone temperature. The platinum basket holding the crucible was hooked by a platinum wire which was inserted into the furnace from the top end of the guiding tube. The experimental set-up and the sample holding technique are displayed in Fig. 3. To verify that equilibration was attained, all samples were equilibrated in the furnace for at least 24 h (Dańczak et al., 2020; Dańczak et al., 2021; Avarmaa et al., 2019; Avarmaa et al., 2020) before being quenched in an ice-water mixture. The experimental procedure has been described in detail in our earlier publications (Klemettinen et al., 2017; Avarmaa et al., 2016).

The quenched samples were dried and mounted in epoxy resin (EpoFix, Struers, Denmark). The sample surfaces were ground, polished, and then carbon coated using a carbon vacuum evaporator (JEOL IB-29510VET). The microstructures were obtained using a Scanning Electron Microscope (SEM; Tescan MIRA 3, Brno, Czech Republic) coupled with an UltraDry Silicon Drift Energy Dispersive X-ray Spectrometer (EDS; Thermo Fisher Scientific, Waltham, MA, USA).

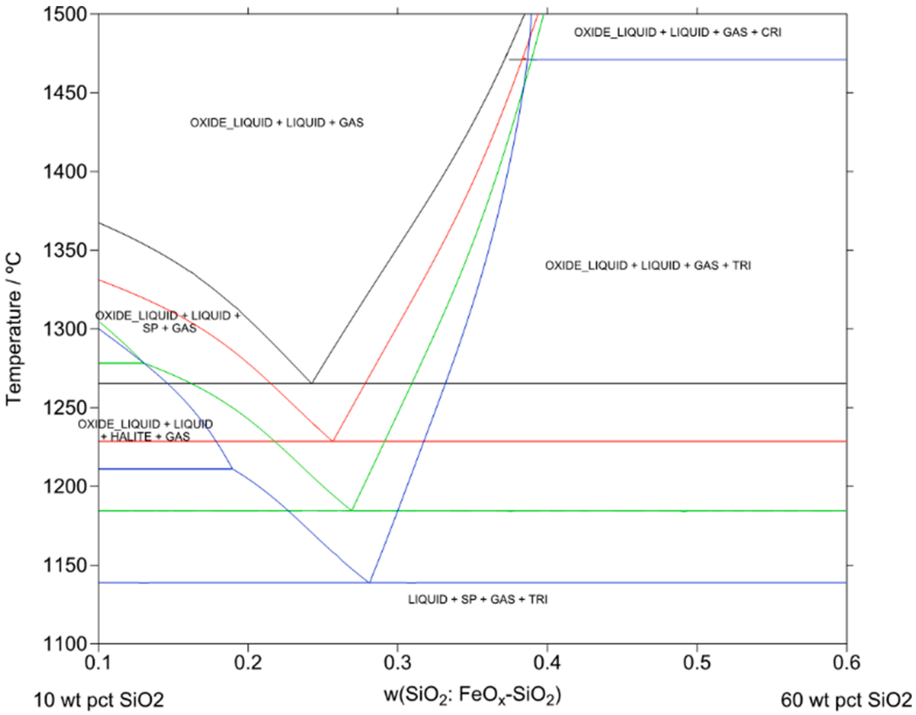

Fig. 2. The isopleths of the Cu-Fe-O-SiO$_2$ system calculated by MTDATA. Blue line-10^{-9} atm; green line-10^{-8} atm; red line-10^{-7} atm; black line-10^{-6} atm (MTOX database (Davies et al., 2002). (For interpretation of the references to colour in this figure legend, the reader is referred to the web version of this article.)

Table 3

The crucibles (primary phases) used and the calculated gas flow rates at 1200–1300 °C for the target P_{O2}.

Temperature/ °C	$Log_{10}P_{O2}$/ atm	Crucible	Gas flow rates/ (mL·min^{-1})		P_{CO2}/ P_{CO}	Fe_2O_3/ SiO_2 weight ratio of slag
			CO_2	CO		
1200	−10	FeO	226.3	73.7	3.1	85/15
	−9	FeO	272.0	28.0	9.7	80/20
	−8	Fe_3O_4	290.5	9.5	30.7	80/20
1250	−10	FeO	177.5	122.5	1.5	85/15
	−9	FeO	246.3	53.7	4.6	85/15
	−8	Fe_3O_4	280.6	19.4	14.5	80/20
	−7	Fe_3O_4	293.6	6.4	45.8	80/20
	−6.5	Fe_3O_4	296.4	3.6	81.5	80/20
1300	−8	FeO	263.3	36.7	7.2	90/10
	−7	Fe_3O_4	287.3	12.7	22.7	90/10
	−6.5	Fe_3O_4	292.7	7.3	40.3	85/15

The concentrations of trace elements in the metal phase as well as the major element compositions of the metal, slag, and magnetite/wüstite phase were obtained with a CAMECA SX100 electron probe microanalyzer (EPMA) using wavelength dispersive spectrometry (WDS) technique. The accelerating voltage and beam current were 20 kV and 60nA, respectively. A defocused beam diameter set to 20 μm for the magnetite/wüstite phase and 50 μm for the metal and slag phases was used. The standard materials used were obsidian for O K$_\alpha$, quartz for Si K$_\alpha$, hematite for Fe K$_\alpha$, and metallic copper for Cu K$_\alpha$, silver for Ag L$_\alpha$, nickel for Ni K$_\alpha$, cobalt for Co K$_\alpha$, and tin for Sn L$_\alpha$. Analytical results were corrected using the PAP on-line correction program (Pouchou and Pichoir, 1986). At least eight points were measured for the metal phase. A three-spot analysis technique was used for the slag and magnetite/wüstite phases, i.e., 24 analyzing spots were selected from the slag/magnetite/wüstite phase and the result for one point was determined by using the average of every three separate analysis spots next to each other. The analytical total of EPMA measurements was within 98–100.7 wt pct. The analyses were taken from areas where all phases were present and in direct contact with each other, examples shown in Fig. 4.

Laser ablation single collector inductively coupled mass spectrometry (LA-ICP-MS) analyses of trace element concentrations in slag and magnetite/monoxide phases were performed at the Geological Survey of Finland (GTK), using a Nu AttoM SC-ICPMS (Nu Instruments Ltd., Wrexham, UK) and an Analyte 193 ArF laser-ablation system (Photon Machines, San Diego, USA). The laser was run at a pulse frequency of 10 Hz and a pulse energy of 5 mJ at 30 % attenuation to produce an energy flux of 2.5 J/cm^2 on the sample surface with a 40 μm spot size. This spot size was chosen to provide the best compromise between adequate resolution, to allow spot analysis of individual phases determined by SEM imaging set at high contrast yet keeping limits of detection (LOD) as low as possible. Each analysis was initiated with a 20 s baseline measurement followed by switching on the laser for 40 s for signal acquisition. The trace element concentrations were obtained using time resolved analysis (TRA) with continuous acquisition of data for each set of points (generally following the scheme of primary standard, quality control standard, 20 unknowns). Both phase analyses of magnetite/wüstite and slag were conducted close to each other from the same well-quenched areas.

For the trace element analyses by LA-ICP-MS, GSE glass was used as the primary external standard, and GSD, BHVO-2G and BCR-2G glasses were used as reference materials for quality control. The isotope ^{57}Fe was used as the internal standard for magnetite/wüstite and ^{29}Si for slag by employing the EPMA measurement results for Fe and Si, respectively. The measurements were performed on isotopes ^{109}Ag for silver, ^{60}Ni for nickel, ^{59}Co for cobalt, and ^{120}Sn for tin at low resolution ($\Delta M/M = 300$) using the fast scanning mode. Data reduction was handled using the GLITTER^{TM} (Van Achterbergh, 2001) software which allows for baseline subtraction, signal integration over a selected time window and quantification using known concentrations of the external and internal standards. The detection limits of EPMA and LA-ICP-MS obtained for this experimental series are listed in Table 4.

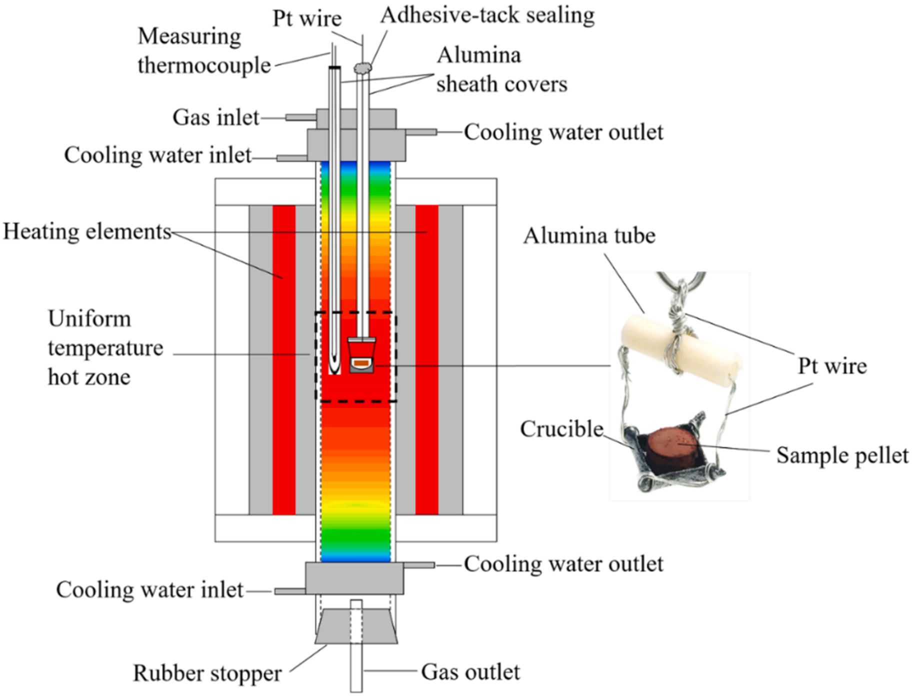

Fig. 3. Schematic of the equilibration furnace and sample holder setup used for the experiments.

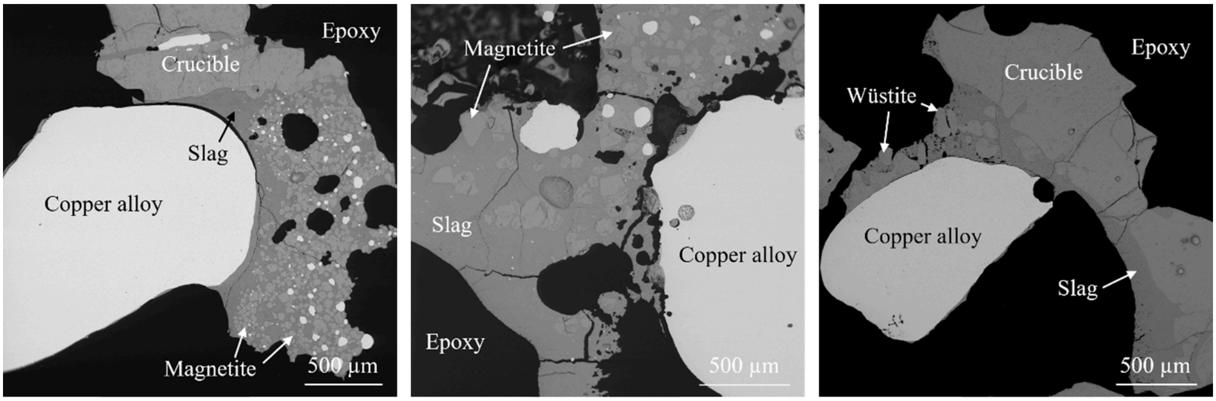

(a) (b) (c)

Fig. 4. Typical microstructures of the copper alloy-slag-magnetite/wüstite equilibria at different temperatures and P_{O2} = 10^{-8} atm; (a) 1200 °C; (b) 1250 °C; (c) 1300 °C.

Table 4
Elemental detection limits of EPMA and LA-ICP-MS analyses obtained in this study/ppmw.

Element	O	Si	Fe	Co	Ni	Cu	Ag	Sn	
EPMA	Copper	437	155	111	120	169	389	232	189
	Slag	692	119	141	206	160	197	196	165
	Magnetite/Wüstite	606	118	158	222	166	199	199	166
LA-HR ICP-MS	Isotope	^{29}Si	^{57}Fe	^{109}Ag	^{60}Ni	^{59}Co	^{120}Sn		
	Slag	7.6	1.1	0.004	0.08	0.01	0.02		
	Magnetite/Wüstite	8.3	1.2	0.004	0.09	0.01	0.03		

3. Results and discussion

The microstructures of samples obtained at 1200–1300 °C and P_{O2} of 10^{-8} atm are shown in Fig. 4. As can be seen in Fig. 4, the copper alloy was equilibrated with molten slag phase and solid magnetite/wüstite, depending on temperature and the prevailing oxygen partial pressure. The fraction of recrystallized magnetite/wüstite phase decreased with increasing oxygen partial pressure. The detailed primary phases of saturation in the slags can be seen in section 3.2.

3.1. *Concentrations of trace elements in copper alloy*

The concentrations of trace elements in copper alloy as a function of P_{O2} are shown in Fig. 5. Fig. 5(a) shows that Ag concentrations in the

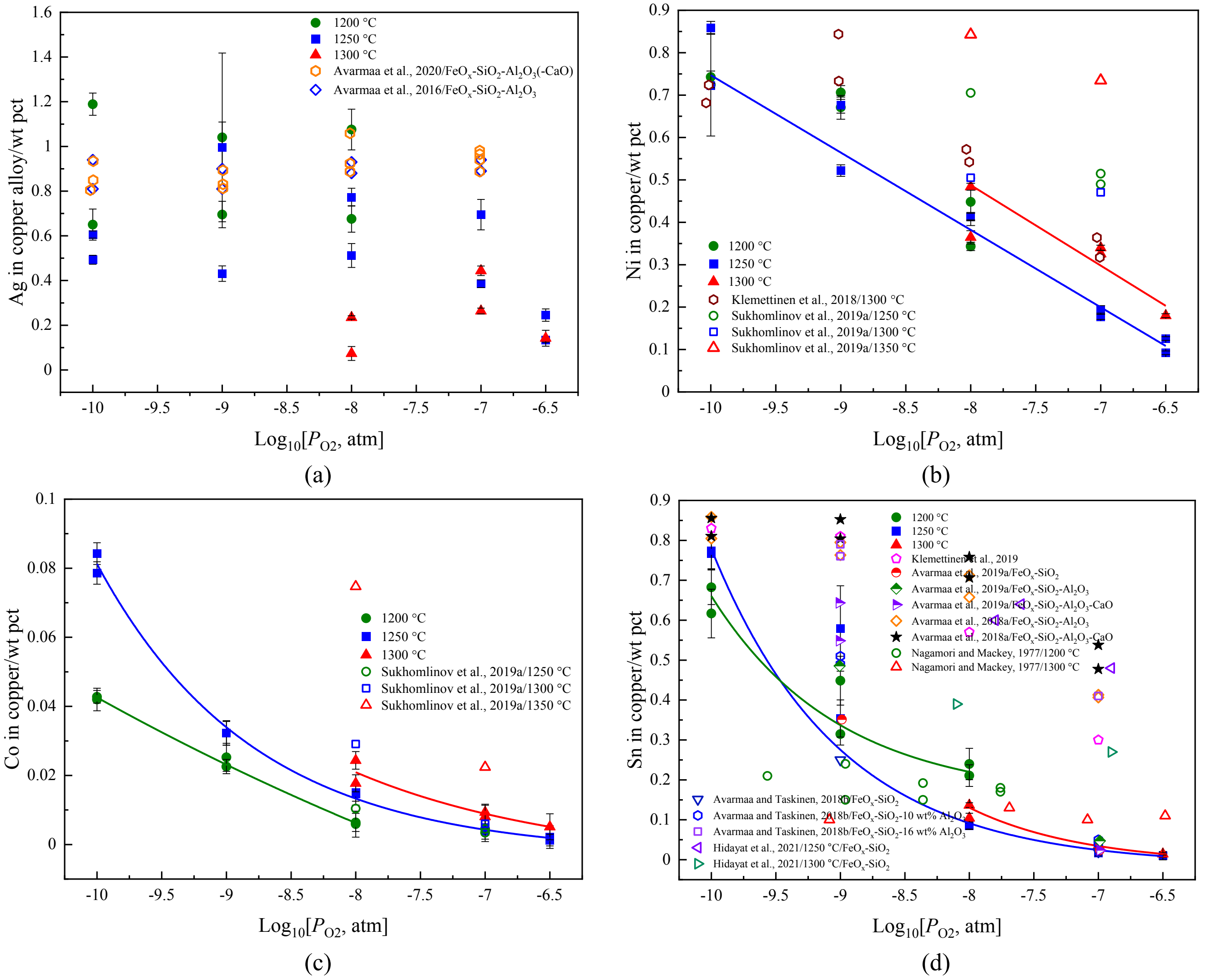

(a) (b) (c) (d)

Fig. 5. Concentrations of Ag (a), Ni (b), Co (c), and Sn (d) in copper alloy as a function of P_{O2} at 1200–1300 °C; Open symbols-results from literature; colored full symbols-present study.

copper alloy were somewhat scattered and had no significant change in the oxygen partial pressure range of 10^{-10}-10^{-8} atm at 1200–1250 °C, whereas it showed a slightly decreasing trend with increasing P_{O2} from 10^{-8} to $10^{-6.5}$ atm at 1250 °C. The results at 1300 °C fluctuated around 0.2 wt pct and at 1200 °C around 1 wt pct. The concentration of Ag in copper alloy decreased from around 1 wt pct to approximately 0.2 wt pct when temperature varied in the range of 1200–1300 °C, indicating a stronger vaporization of Ag at higher temperatures. The decreasing impact of higher temperature on the deportment of Ag into copper alloy was also observed by Sukhomlinov *et al.* (Sukhomlinov et al., 2019a). The results by Avarmaa *et al.* (Avarmaa et al., 2020; Avarmaa et al., 2016) were almost constant at 0.9 wt pct at P_{O2} of 10^{-10}-10^{-7} atm, similar to the present results obtained at 1200 °C. In another study by Avarmaa *et al.* (Avarmaa et al., 2019), the concentration of Ag in copper alloy equilibrated with silica-saturated slags was approximately 0.2–0.3 wt%, close to the present results at 1300 °C.

Fig. 5(b) shows that concentration of Ni in the copper alloy had a linearly decreasing trend with increasing P_{O2} at all temperatures investigated. With increasing temperature from 1250 °C to 1300 °C, the concentration of Ni in copper alloy increased by approximately 0.1 wt pct. The present results for Ni in copper alloy were lower than the observations by Klemettinen *et al.* (Klemettinen et al., 2018) and Sukhomlinov *et al.* (Sukhomlinov et al., 2019a) but showed similar decreasing trends.

Co displayed the lowest concentration in the copper alloy when compared with other trace elements investigated in this study, as shown in Fig. 5(c). Co concentration in the copper alloy had a downward trend with increasing P_{O2}, as reported in previous studies (Dańczak et al., 2020; Sukhomlinov et al., 2019a). However, the decreasing trend was less vigorous at higher P_{O2}. The increase of temperature favored the deportment of Co in the copper alloy. The results by Sukhomlinov *et al.* (Sukhomlinov et al., 2019a) were within the range observed in the present study but were significantly lower than the data by Dańczak *et al.* (Dańczak et al., 2020).

The trend line for Sn in copper alloy exhibited a similar decreasing trend as Co. However, the impact of temperature was not as strong as for the other trace elements. The present results of Sn in copper alloy equilibrated with magnetite/wüstite-saturated slags were somewhat lower than the observations (Avarmaa et al., 2018a, 2019; Dańczak et al., 2021; Hidayat et al., 2021; Klemettinen et al., 2019; Avarmaa and Taskinen, 2018b) obtained from copper alloy in equilibrium with silica/(Al-Fe) spinel-saturated slags, which showed different downward trends. However, the results by Avarmaa *et al.* (Avarmaa et al., 2019) determined from the copper alloy in equilibrium with silica-saturated slags were close to the present results at 1250 °C. The present results obtained at 1200 °C were slightly higher than the data by Nagamori and

Mackey (Nagamori and Mackey, 1977) in the P_{O2} range of 10^{-10} to 10^{-8} atm, whereas the present results at 1300 °C were lower than their data (Nagamori and Mackey, 1977) by approximately 0.1 wt pct. The impacts of CaO, Al_2O_3, and MgO on increasing the Sn concentration in copper alloy were reported in literature (Avarmaa et al., 2018a; Dańczak et al., 2021; Avarmaa and Taskinen, 2018b).

3.2. Concentrations of trace elements in Magnetite/Wüstite

The loss of trace elements in the solid magnetite/wüstite primary phase in the copper-slag-magnetite/wüstite-gas equilibria system was investigated by LA-ICP-MS for the first time in the present study, as shown in Fig. 6. Fig. 6(a) indicates that the dissolution of Ag to the magnetite/wüstite phase was extremely low (<1ppm), compared with the other trace elements. The results for Ni, Co, and Sn displayed a similar increasing trend with increasing P_{O2}, wherein the loss of Ni and Co in the magnetite/wüstite phase were higher than that of Sn. The effect of higher temperature on decreasing the concentration of trace elements in magnetite/wüstite was evident for all minor elements, although less clear for Ag between 1250 and 1300 °C. The phenomenon of trace element dissolutions in solid phase, i.e., in magnetite/wüstite in the present study, was not observed in our previous studies (Avarmaa et al., 2019; Sukhomlinov et al., 2019a) focusing on the copper alloy/slag/tridymite equilibria system.

3.3. Concentrations of trace elements in slag

The concentrations of trace elements in the slag by LA-ICP-MS with their standard deviations (±1σ) against P_{O2} are presented in Fig. 7. Fig. 7 (a) indicates the concentration of Ag in all magnetite/wüstite-saturated slags in equilibrium with copper alloy was lower than 70 ppm, suggesting a strong deportment of Ag into the copper alloy phase, when combined with above mentioned low Ag concentrations in magnetite/wüstite. The results at all temperatures investigated increased with increasing P_{O2}. The increase of temperature reduced the loss of Ag in the slag to varying degrees, depending on the P_{O2}. The data by Avarmaa *et al.* (Avarmaa et al., 2016) for silver at Al-Fe spinel saturation were higher than the present results and the observations in literature (Sukhomlinov et al., 2019a), but they displayed a similar increasing trend with increasing P_{O2}. The Ag concentrations in slag reported by Hidayat *et al.* (Hidayat et al., 2019) had some scatter but were within the range of present observations. Additionally, it was reported in the study (Avarmaa et al., 2020) that the loss of Ag in slag can be reduced by adding CaO into the iron silicate slag.

The observed concentration of Ni in slag, as shown in Fig. 7(b), increased throughout the P_{O2} range investigated at all temperatures, as have been reported in literature (Dańczak et al., 2021; Sukhomlinov et al., 2019a; Klemettinen et al., 2018). The present results for Ni in the slag decreased with increasing temperature at fixed P_{O2}, contrary to the

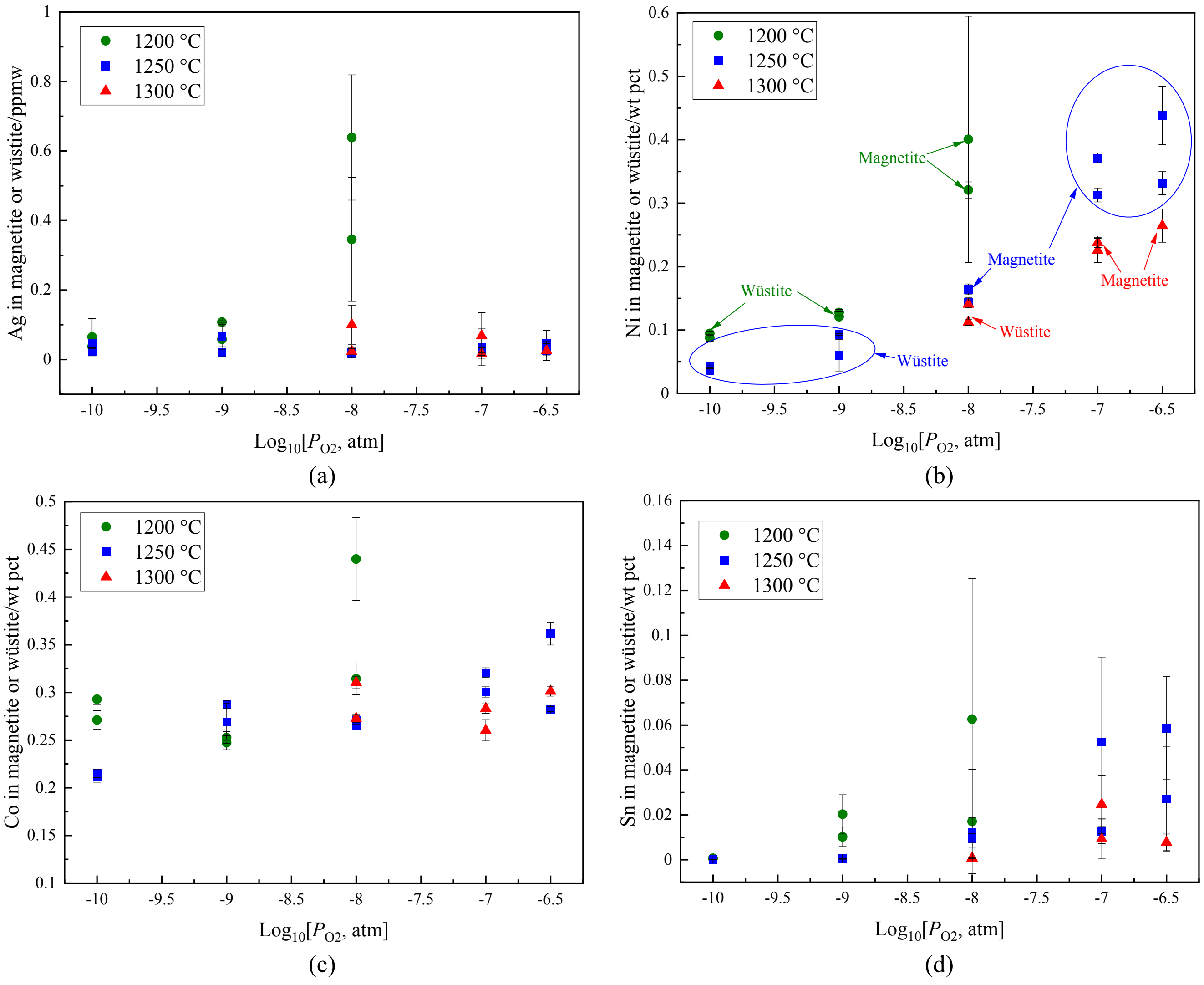

(a) (b) (c) (d)

Fig. 6. Concentrations of trace elements in magnetite/wüstite *vs.* P_{O2} at 1200–1300 °C; Ag (a), Ni (b), Co (c), and Sn (d).

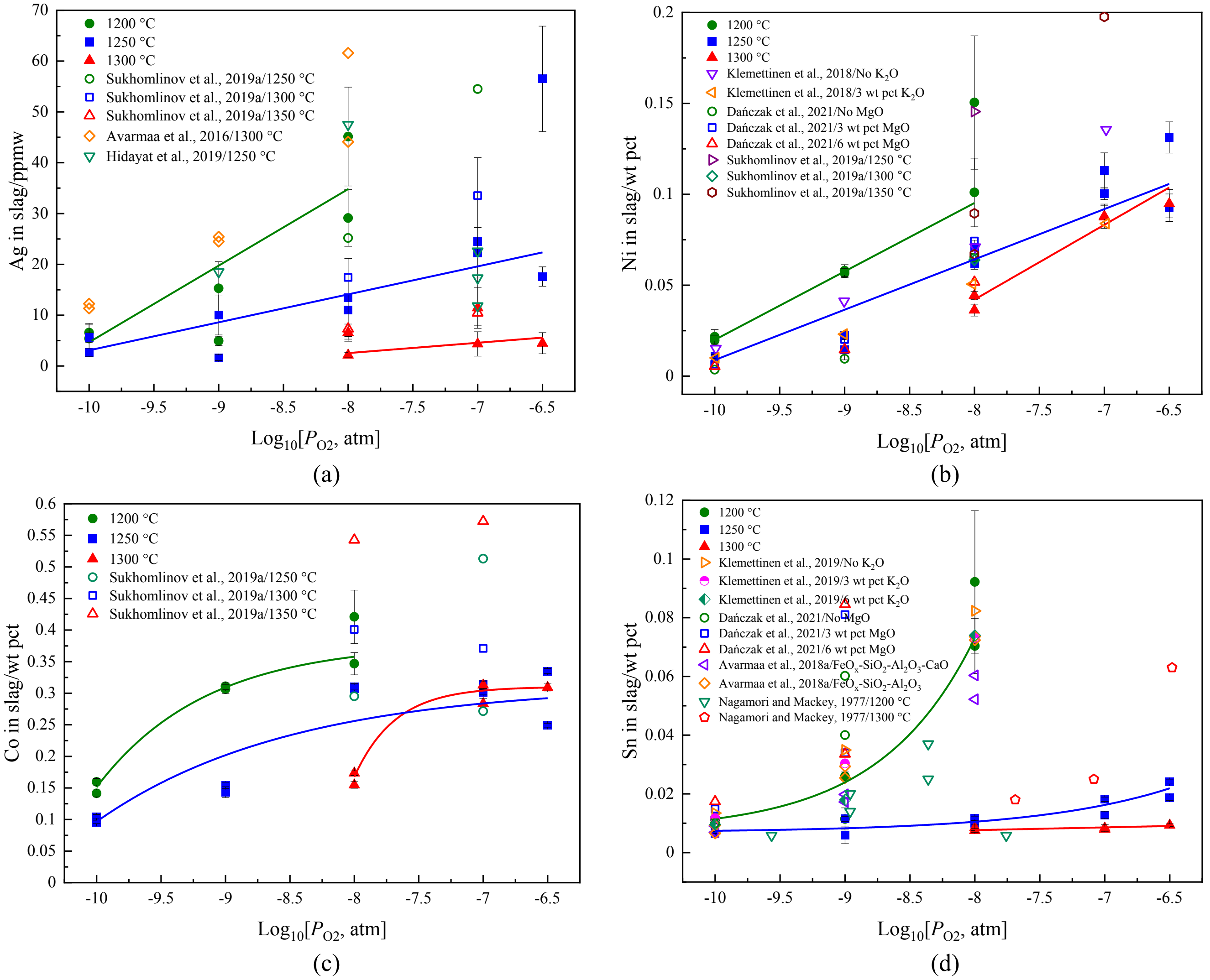

Fig. 7. Trace element concentrations in FeO_x-saturated slag as a function of P_{O2} at 1200–1300 °C; Ag (a), Ni (b), Co (c), and Sn (d).

findings by Sukhomlinov *et al.* (Sukhomlinov et al., 2019a). The discrepancies might attribute to the strong dissolution of Ni in magnetite/wüstite. The Ni concentration in slag measured by Klemettinen *et al.* (Klemettinen et al., 2018) and Dańczak *et al.* (Dańczak et al., 2021) at 1300 °C increased approximately from 300 ppm to 0.13 wt pct along with increasing P_{O2}, which is close to the present results obtained at 1250–1300 °C. They also reported that K_2O and MgO additions in the iron silicate-based slag decreased the loss of Ni in slag.

Fig. 7(c) indicates that the concentration of Co in the slag displayed a non-linear but increasing trend with increasing P_{O2}. However, the slope was steeper at P_{O2} lower than 10^{-8} atm at 1200–1250 °C and at 1300 °C below 10^{-7} atm. The influence of higher temperature on decreasing the Co concentration in slag was more significant in the lower P_{O2} range of 10^{-10} to 10^{-8} atm. A contradictory impact of temperature on Co loss in slag was observed by Sukhomlinov *et al.* (Sukhomlinov et al., 2019a). Reddy *et al.* (Reddy and Healy, 1981) reported that the solubility of Co in Cu_2O-CoO-SiO_2 slags increased with increasing ratios of Cu_2O/SiO_2, metal-to-oxide and the concentration of Co in the alloy, which fits well with the observations by Derin and Yücel (Derin and Yücel, 2002) for the solubility of Co in FeO_x-SiO_2-Al_2O_3 slags. The concentrations of Co in the MgO-containing slag reported by Dańczak *et al.* (Dańczak et al., 2020) were around 30–70 ppm, which are much lower than the present results.

As shown in Fig. 7(d), concentration of Sn in the slag increased significantly with increasing P_{O2} at 1200 °C. However, the results obtained at 1250–1300 °C had no significant changes over the entire P_{O2} range studied. The increase of temperature from 1200 °C to 1250 °C reduced the Sn concentration in slag substantially at P_{O2} higher than 10^{-10} atm, owing to its stronger volatilization at more oxidizing conditions (Avarmaa et al., 2019), whereas temperature influenced much less on the Sn concentration between 1250 °C and 1300 °C. The present results at 1200 °C were slightly higher than the data by Nagamori and Mackey (Nagamori and Mackey, 1977), but at 1300 °C the present results were on the lower side of their observations obtained in the same conditions. The results reported by Hidayat *et al.* (Hidayat et al., 2021) ranged from 580 ppm to 0.45 wt pct and 528 ppm to 1.33 wt pct, at 1250 and 1300 °C, respectively, which are on higher side of the present observations. It was also reported in literature (Anindya et al., 2013; Avarmaa et al., 2018a; Dańczak et al., 2021; Klemettinen et al., 2019) that additions of K_2O, MgO, and CaO into iron silicate slags depressed the loss of Sn into slags.

3.4. Distribution coefficients between copper alloy and slag

The high-temperature equilibrium reactions of a trace element *Me* between molten copper and slag in WEEE processing can be described using the following equation:

$$Me+\frac{v}{2}O_2=MeO_v \tag{1}$$

where the valence of trace element *Me* in slag equals to 2ν. The equilibrium reaction constant *K* for reaction (1) can be defined as:

$$K = \frac{a(MeO_\nu)}{a[Me]P_{O_2}^{\nu/2}} \tag{2}$$

where $a[Me]$ and $a(MeO_\nu)$ refer to the activities of *Me* and MeO_ν in the copper alloy and slag, respectively. The distribution coefficient of Me between copper alloy and slag can be defined as:

$$L_{Me}^{Cu/S} = \frac{[wtpctMe]_{incopperalloy}}{(wtpctMe)_{inslag}} \tag{3}$$

where $[wt\,pct\,Me]$ and $(wt\,pct\,Me)$ denote the concentrations of trace element in copper alloy and slag, respectively. As suggested by Takeda *et al.* (Takeda et al., 1983), the distribution coefficient can be expressed further as:

$$L_{Me}^{Cu/S} = \frac{[n_T]_{incopperalloy}(\gamma_{MeO_\nu})P_{O_2}^{-\nu/2}}{K[\gamma_{Me}](n_T)_{inslag}} \tag{4}$$

where *K* represents the equilibrium constant of equation (1) and n_T represents the total mole number of mono-cationic constituents in 100 g copper alloy and slag. $[\gamma_{Me}]$ and $(\gamma_{MeO\nu})$ denote the activity coefficients of Me in copper alloy phase and MeO_ν in slag phase, respectively. By reorganizing equation (4), the logarithmic distribution coefficient can be represented as:

$$Log_{10}L_{Me}^{Cu/S} = Log_{10}\frac{(\gamma_{MeO_\nu})[n_T]_{incopperalloy}}{K(n_T)_{inslag}[\gamma_{Me}]} - \frac{\nu}{2}Log_{10}P_{O_2} \tag{5}$$

As the concentration of *Me* in the copper alloy and MeO_ν in the slag are quite low, thus obeying Henry's law, the $Log_{10}\frac{(\gamma_{MeO_\nu})[n_T]_{incopperalloy}}{K(n_T)_{inslag}[\gamma_{Me}]}$ can be regarded as a constant at a fixed temperature. $-\frac{\nu}{2}$ is the slope of the linearly fitted relationship between $Log_{10}L_{Me}^{Cu/S}$ and $Log_{10}P_{O_2}$ which can be used to determine the oxidation state of trace element *Me* in slag. The calculated logarithmic distribution coefficients of trace elements between copper alloy and slag as a function of logarithmic P_{O2} are displayed in Fig. 8. The present experimental results were also compared with the data from literature.

Compared with the other trace elements investigated in this study, the logarithmic distribution coefficient of Ag in Fig. 8(a) is rather

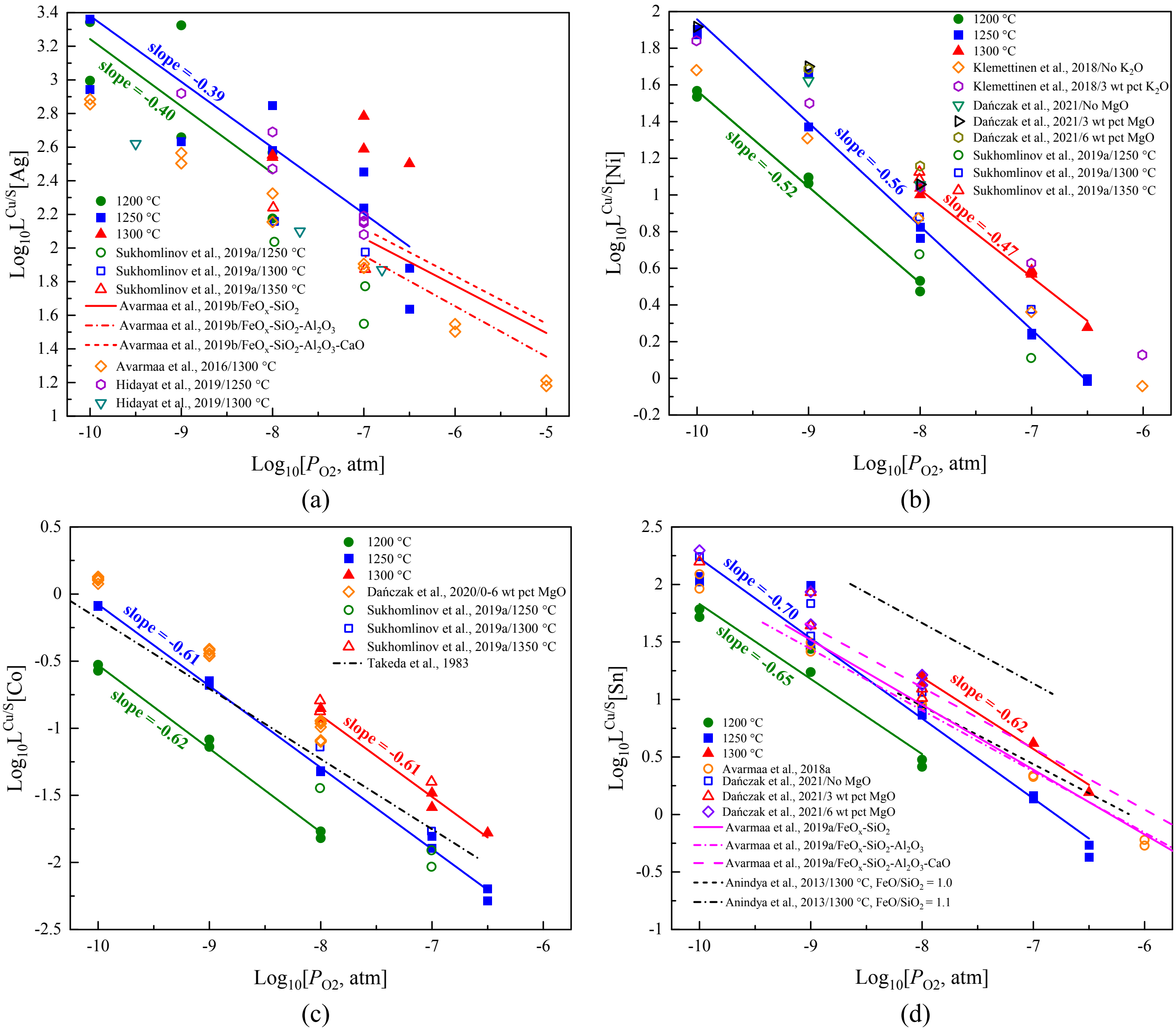

Fig. 8. Logarithmic distribution coefficients of trace elements between copper alloy and slag *vs.* P_{O2} at 1200–1300 °C and FeO$_x$ saturation; Ag (a), Ni (b), Co (c), and Sn (d).

scattered, ranging from 1.6 to 3.4 at 1200–1300 °C and P_{O2} of $10^{-6.5}$-10^{-10} atm. This suggests that Ag was highly accumulated in the copper alloy. The present distribution coefficient values at 1200–1250 °C decreased with increasing P_{O2}, as reported by Sineva *et al.* (Sineva et al., 2021); however, the results obtained in this study at 1300 °C remained almost constant around 2.6. The logarithmic distribution coefficient of Ag increased by approximately 0.2 units with increasing temperature from 1200 °C to 1250 °C. A depressing impact of higher temperature on $L_{Ag}^{Cu/S}$ was determined by Hidayat *et al.* (Hidayat et al., 2019), contrary to the observations by Sukhomlinov *et al.* (Sukhomlinov et al., 2019a). The present results at 1200 °C were on the high side of the data between molten copper and Al-Fe spinel saturated slag at 1300 °C determined by Avarmaa *et al.* (Avarmaa et al., 2016) at hercynite-magnetite saturation. The logarithmic distribution coefficients of Ag between copper alloy and silica-saturated iron silicate slags reported by Avarmaa *et al.* (Avarmaa et al., 2019) at 1300 °C were close to the present extrapolated results at 1250 °C. In another study by Avarmaa *et al.* (Avarmaa et al., 2020), the distribution coefficient of Ag increased with addition of CaO into slag. As for the dissolution mechanism of Ag in slags, some researchers suggested $AgO_{0.5}$ (Ag^{+}) (Avarmaa et al., 2019; Kashima et al., 1978; Sukhomlinov et al., 2019a; Takeda et al., 1983; Park and Min, 1999) in slags. Avarmaa *et al.* (Avarmaa et al., 2020; Avarmaa et al., 2016) and Hidayat *et al.* (Hidayat et al., 2019) proposed a mixed valence of Ag^{+} and Ag^{2+}. The slopes of the trend lines at 1200 °C and 1250 °C in this study were −0.40 and −0.39, respectively, giving an indication that Ag oxide dissolves in the slag with a combination valence of 1 + and 2+, similar to the observations by Avarmaa *et al.* (Avarmaa et al., 2020; Avarmaa et al., 2016) and Hidayat *et al.* (Hidayat et al., 2019).

The distribution coefficient of Ni in Fig. 8(b) decreased with increasing P_{O2} over the entire P_{O2} range studied. The increase of temperature from 1200 to 1300 °C favored the deportment of Ni into copper alloy, in good agreement with the observations by Sukhomlinov *et al.* (Sukhomlinov et al., 2019a). The present results at 1300 °C were slightly higher than the data by Klemettinen *et al.* (Klemettinen et al., 2018), which were determined between copper alloy and K_2O-free slags, but they fit well with their results for slag containing 3 wt% K_2O. The results by Dańczak *et al.* (Dańczak et al., 2021) were slightly higher compared with the present and other studies (Sukhomlinov et al., 2019a; Klemettinen et al., 2018). Klemettinen *et al.* (Klemettinen et al., 2018) observed that addition of K_2O into Al-Fe spinel saturated iron silicate slags increased the distribution coefficient of Ni between copper alloy and slag. The slope of the current trend lines at 1200–1300 °C was approximately −0.5, indicating that Ni dissolved into the slag as divalent oxide NiO, which agrees well with the results of previous studies (Kaur et al., 2009; Sukhomlinov et al., 2019a; Takeda et al., 1983; Wang et al., 1973, 1974). Reddy and Acholonu (Reddy and Acholonu, 1984) proposed that Ni dissolved in Al-Fe spinel saturated fayalite slags as a combination of Ni^{2+} and Ni^{0}.

As shown in Fig. 8(c), the distribution coefficient of Co between copper alloy and slag decreased with increasing P_{O2} at all temperatures investigated. The logarithmic values of the present distribution coefficients were below zero, suggesting that Co was markedly accumulated in the slag phase. The distribution coefficient of Co decreased around 0.5 and 0.4 log units with increasing temperature from 1200 °C to 1250 °C and from 1250 °C to 1300 °C, respectively, at P_{O2} of 10^{-8} atm. Similar impact of temperature was also observed by Sukhomlinov *et al.* (Sukhomlinov et al., 2019a). The results by Dańczak *et al.* (Dańczak et al., 2020) were intermediate between the present results at 1250 °C and 1300 °C. The present results at 1250 °C generally fitted well with the trend line by Takeda *et al.* (Takeda et al., 1983). The slopes of the trend lines of the present results at 1200–1300 °C were around −0.60. This indicated that Co in the slag existed as a combination of Co^{2+} and Co^{3+}, as the species CoO and Co_2O_3 would have slopes of 0.5 and 0.75, respectively. However, in most previous studies (Dańczak et al., 2020; Derin and Yücel, 2002; Kho et al., 2006; Reddy and Healy, 1981a,b, Ren et al., 2020, 2021; Sukhomlinov et al., 2019a; Takeda et al., 1983; Teague et al., 2001; Yazawa, 1980; Sukhomlinov and Taskinen, 2017), Co was suggested to exist as a divalent oxide species of CoO.

Similar to the present results for Ni and Co, the distribution coefficient of Sn between copper alloy and slag displayed a decreasing trend with increasing P_{O2}. Moreover, a higher temperature favored the deportment of Sn into the copper alloy phase, as reported by Nagamori and Mackey (Nagamori and Mackey, 1977). The results by Avarmaa *et al.* (Avarmaa et al., 2018a) at Al-Fe spinel saturation were close to the present data at 1250 °C, whereas the data between copper alloy and silica-saturated iron silicate slags by Avarmaa et al. (Avarmaa et al., 2019) are intermediate between the present results at 1250 °C and 1300 °C. It was reported by Dańczak *et al.* (Dańczak et al., 2021) at Al-Fe spinel saturation that the distribution coefficient of Sn increased with increasing the concentration of MgO in slags. Anindya *et al.* (Anindya et al., 2013) observed that the FeO/SiO_2 ratio and CaO content in slags had strong impacts on the distribution coefficient of Sn. They found that the logarithmic distribution coefficient of Sn increased by approximately 0.8 with increasing the FeO/SiO_2 ratio from 1.0 to 1.1 and CaO content from 13.8 wt pct to 21.9 wt pct (Anindya et al., 2013). The slopes of the trend lines determined by Anindya *et al.* (Anindya et al., 2013) were close to −0.5 and they suggested that tin was present in slags as SnO. In the present study, the slopes of the trend lines at 1200–1300 °C were from −0.6 to −0.7, which suggested that tin in slags had a mixed valence of 2 + and 4+, since the species SnO and SnO_2 would have slopes of 0.5 and 1, respectively. Takeda *et al.* (Takeda et al., 1983) observed that tin preferred to concentrate in calcium ferrite slag when compared with iron silicate slag. In addition, they described that tin in calcium ferrite slags presented as SnO_2 at P_{O2} higher than 10^{-8} atm (Takeda et al., 1983). Avarmaa *et al.* (Avarmaa et al., 2018a) proposed that tin had a mixed valence in the Al-Fe spinel saturated FeO_x-SiO_2-Al_2O_3 slag but presented as $SnO_{1.5}$ in the FeO_x-SiO_2-Al_2O_3-CaO slag at 1300 °C and P_{O2} of 10^{-7} to 10^{-5} atm. They also reported that tin presented as SnO in both slags over the P_{O2} range of 10^{-10} to 10^{-8} atm. Starykh *et al.* (Starykh et al., 2021) investigated the phase equilibria of the Fe-free Cu-Sn-Si-O system at 1180–1665 °C with tridymite/cuprite/cristobalite saturation in slags. They reported that tin existed as SnO and SnO_2 in slags and the total amount of tin oxide in slags decreased with increasing temperature. The loss of tin is similar to the present observations where more than 80 % was vaporized at high oxygen partial pressures at 1250 and 1300 °C during the equilibration.

3.5. Distribution coefficients between Magnetite/Wüstite and slag

As described in sections 3.2 and 3.3, trace elements dissolved into the solid magnetite/wüstite and molten slag phases to varying degrees. To have a deeper understanding of the trace element distribution mechanism in secondary copper smelting, the logarithmic distribution coefficients of trace elements between the solid magnetite/wüstite phase and molten slag were calculated and presented in Fig. 9 as a function of logarithmic P_{O2}.

Fig. 9(a) indicates that Ag preferred the slag phase when compared with the solid magnetite/wüstite and the distribution coefficients at 1250–1300 °C decreased with increasing P_{O2}. The logarithmic distribution coefficient results at 1200 °C showed constant value around −2. The increase of temperature from 1250 to 1300 °C increased the distribution coefficient of Ag by approximately 0.6 log units.

As can be seen in Fig. 9(b), Ni distributed 2–4 times more in the solid magnetite/wüstite phase than in the molten slag. The distribution coefficient of Ni between magnetite/wüstite and slag at all temperatures investigated had a decreasing trend first and then increased with increasing P_{O2}. Co displayed similar trends as Ni, however, Co distributed more into the slag phase at a certain P_{O2} which was depended on the experimental temperature employed.

Fig. 9(d) suggests that the distribution coefficient of Sn increased with increasing P_{O2} at all temperatures. A higher temperature favored

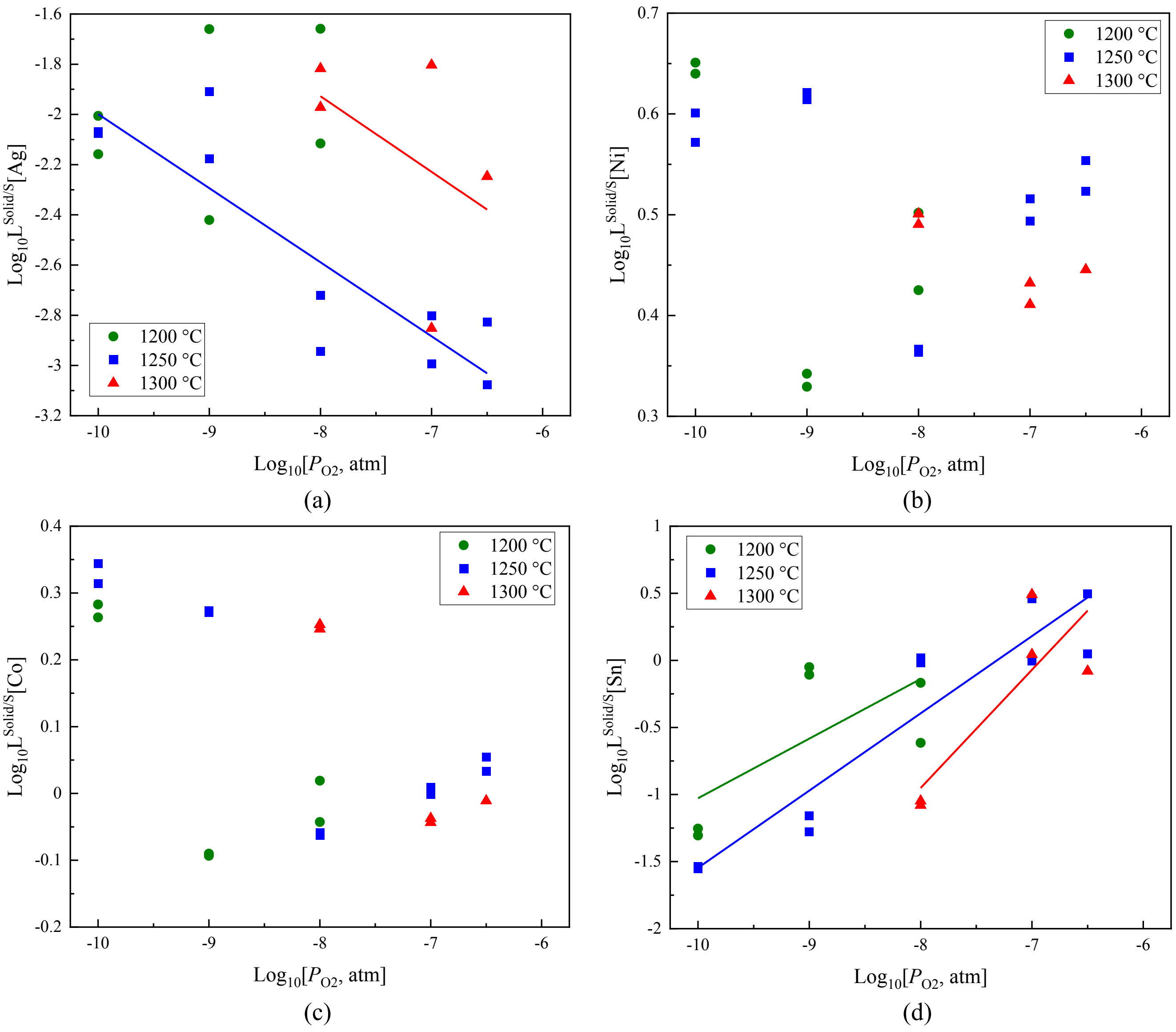

Fig. 9. Logarithmic distribution coefficients of trace elements between solid magnetite/wüstite and slag *vs.* P_{O2} at 1200–1300 °C and FeO_x saturation; Ag (a), Ni (b), Co (c), and Sn (d).

the distribution of Sn into slag than into magnetite/wüstite. Furthermore, Sn distributed more into the molten slag phase at lower P_{O2}, depending on temperature.

The distribution of trace element between molten slag and solid magnetite/wüstite can be described by equilibrium reaction (6):

$$(MeO_n) + \frac{v}{2}O_2 = [MeO_{n+v}] \tag{6}$$

where (MeO_n) and $[MeO_{v+n}]$ represent the oxides of trace element in slag and magnetite/wüstite, respectively. Similar to the calculation for the logarithmic distribution coefficient of a trace element between copper alloy and slag, the logarithmic distribution coefficient of a trace element between magnetite/wüstite and slag can be expressed as:

$$Log_{10}L_{Me}^{Solid/S} = A + \frac{v}{2}Log_{10}P_{O_2} \tag{7}$$

where A is a constant at a given temperature. The slope, $v/2$, of the trend line for the logarithmic distribution coefficient of a trace element between magnetite/wüstite and slag as a function of logarithmic P_{O2} can be used to evaluate the change of valence for trace elements during their distributions between magnetite/wüstite and slag. If the trace element in slag is reduced to a lower valence state in magnetite/wüstite, the slope $v/2$ should be negative, i.e., the logarithmic distribution coefficient of trace element between magnetite/wüstite and slag decreased with increasing logarithmic P_{O2}. On the contrary, if the trace element distributes increasingly into the magnetite/wüstite by further oxidizing the trace element species from slag, the slope should be positive, i.e., the logarithmic distribution coefficient of trace element increases with increasing P_{O2}.

Fig. 9(a) indicates that Ag was reduced to a lower valence state in magnetite/wüstite from the molten slag, independently of the slag saturation phase. In contrast, Sn was oxidized to higher valence states from the molten slag phase to magnetite/wüstite. It dissolves in iron spinels as Sn^{4+} in the octahedral sites (Berry et al., 1998). Thus, the mixed tetra- and divalent tin oxide in the slag (Avarmaa et al., 2018a, 2019; Klemettinen et al., 2019) is predominantly divalent in wüstite (FeO), and tetravalent in magnetite (Fe_3O_4). As for Ni and Co in the solid phases, both of them were reduced to lower-valent oxide species (MeO) from the molten slag when the slag was saturated with wüstite. However, they were oxidized further to higher valent species when the slag was saturated with magnetite which indicates the fact that cobalt and nickel (inverse spinels) in ferrite can dissolve both in octahedral and tetrahedral sites (Lu and Dieckmann, 1995; Salazar-Tamayo et al., 2019) as divalent and trivalent species. Fig. 9(b) and 9(c) suggest that a higher temperature favored the deportment of Ni and Co into wüstite but depressed their distributions into magnetite.

4. Conclusions

With a purpose of exploring the potential of recycling valuable metals from WEEE through secondary copper smelting and finding the optimal fluxing practices, the distributions of selected trace elements (Ag, Ni, Co, and Sn) between copper alloy and magnetite/wüstite-saturated iron silicate slags were investigated at 1200–1300 °C and P_{O2} of 10^{-10} to$10^{-6.5}$ atm using the high-temperature equilibration followed by drop-quench technique and in situ phase composition analyses.

It was found that silver was highly deported into the copper alloy, however, cobalt markedly distributed into the slag and magnetite/wüstite phases. Nickel and tin mainly deported into the copper alloy at lower P_{O2}, depending on the temperature. The distributions of all trace elements between copper alloy and slag investigated in this study were highly dependent on P_{O2} and temperature, and generally decreased with increasing P_{O2} and decreasing temperature which indicates that they dissolved in the slag as oxides.

By comparison of present results at magnetite/wüstite saturation in slag and the previous data (Avarmaa et al., 2018a; Katri Avarmaa et al., 2019; K. Avarmaa et al., 2019; Dańczak et al., 2021; Hidayat et al., 2019; Sukhomlinov et al., 2019a; Avarmaa et al., 2016) at Al-Fe spinel/silica-saturation, it can be concluded that the type of slag saturation has a small impact on the distribution coefficients of trace element between copper alloy and slag. Cobalt and nickel concentrations in magnetite and wüstite were high and they favored the solid phases compared to their dissolution concentrations in slag. The trace element distribution measurements in the magnetite and wüstite phases also indicated that their speciations are different in the slag and the solid oxide primary phases. The present results indicate that the trace elements from WEEE can be effectively recovered into the copper alloy through secondary copper smelting route and their recoveries can be improved by increasing temperature and lowering P_{O2}.

From the perspective of industrial practices, e.g., the WEEE processing in a TSL furnace, the improvement of the recoveries of trace elements can be handled by adjusting the injection of fuel to air/oxygen ratio into the furnace through the submerged lance. The present observations also confirmed the substantial vaporization tendencies of some trace elements reported earlier (Avarmaa et al., 2019; Starykh et al., 2021).

CRediT authorship contribution statement

Min Chen: Conceptualization, Investigation, Methodology, Software, Data curation, Writing–original draft. **Katri Avarmaa:** Methodology, Supervision, Validation, Writing–review & editing. **Pekka Taskinen:** Methodology, Software, Supervision, Validation, Writing–review & editing. **Lassi Klemettinen:** Data curation, Writing–review & editing. **Radoslaw Michallik:** Writing–review & editing. **Hugh O'Brien:** Writing–review & editing. **Ari Jokilaakso:** Supervision, Project administration, Resources, Validation, Funding acquisition, Writing–review & editing.

Declaration of Competing Interest

The authors declare that they have no known competing financial interests or personal relationships that could have appeared to influence the work reported in this paper.

Acknowledgements

This study received financial support from Aalto University, School of Chemical Engineering and Business Finland funded SYMMET program (grant number 3891/31/2018). The utilization of the Academy of Finland's RawMatTERS Finland Infrastructure (RAMI) based at Aalto University, GTK in Espoo, and VTT in Espoo is appreciated. Min Chen is grateful for the China Scholarship Council (grant number 201806370217) for a doctoral project grant.

References

Marinello, S., Gamberini, R., 2021. Multi-criteria decision making approaches applied to waste electrical and electronic equipment (WEEE): a comprehensive literature review. Toxics 9 (1), 13. https://doi.org/10.3390/toxics9010013.

Ibanescu, D., Cailean, D., Teodosiu, C., Fiore, S., 2018. Assessment of the waste electrical and electronic equipment management systems profile and sustainability in developed and developing European Union countries. Waste Manage. 73, 39–53. https://doi.org/10.1016/j.wasman.2017.12.022.

Directive 2012/19/EU of the European Parliament and of the Council of 4 July 2012 on waste electrical and electronic equipment, WEEE. Official Journal of the European Union L, 197, 38-71. Accessed at: https://eur-lex.europa.eu/legal-content/EN/TXT/PDF/?uri=CELEX:32012L0019&from=EN.

Messmann, L., Helbig, C., Thorenz, A., Tuma, A., 2019. Economic and environmental benefits of recovery networks for WEEE in Europe. J. Cleaner Prod. 222, 655–668. https://doi.org/10.1016/j.jclepro.2019.02.244.

Zhang, L., Xu, Z., 2016. A review of current progress of recycling technologies for metals from waste electrical and electronic equipment. J. Cleaner Prod. 127, 19–36. https://doi.org/10.1016/j.jclepro.2016.04.004.

Wang, M., Tan, Q., Chiang, J.F., Li, J., 2017. Recovery of rare and precious metals from urban mines-A review. Frontiers of Environmental Science & Engineering 11 (5), 1–17. https://doi.org/10.1007/s11783-017-0963-1.

Cesaro, A., Marra, A., Kuchta, K., Belgıorno, V., Van Hullebusch, E.D., 2018. WEEE management in a circular economy perspective: An overview. Global NEST Journal 20, 743–750.

Cui, J., Zhang, L., 2008. Metallurgical recovery of metals from electronic waste: A review. J. Hazard. Mater. 158 (2–3), 228–256. https://doi.org/10.1016/j.jhazmat.2008.02.001.

Yazawa, A., 1980. Distribution of various elements between copper, matte and slag. Erzmetall 33 (7–8), 377–382.

Zeng, X., Mathews, J.A., Li, J., 2018. Urban mining of e-waste is becoming more cost-effective than virgin mining. Environ. Sci. Technol. 52 (8), 4835–4841. https://doi.org/10.1021/acs.est.7b04909.

Shuva, M.A.H., Rhamdhani, M.A., Brooks, G.A., Masood, S., Reuter, M.A., 2016. Thermodynamics data of valuable elements relevant to e-waste processing through primary and secondary copper production: a review. J. Cleaner Prod. 131, 795–809. https://doi.org/10.1016/j.jclepro.2016.04.061.

Lehner, T. (1999). Integrated recycling of non-ferrous metals at Boliden Ltd., Rönnskär smelter. In: Proceedings of IEEE International Symposium on Electronics and the Environment, Oak Brook, IL, USA, pp. 42-47.

Veldhuizen, H., Sippel, B., 1994. Mining discarded electronics. *Industry and Environment.* 17 (3), 7–11.

Hagelüken, C., 2006. Recycling of electronic scrap at Umicore's integrated metals smelter and refinery. Erzmetall 59 (3), 152–161.

Hagelüken, C., Corti, C.W., 2010. Recycling of gold from electronics: Cost-effective use through 'Design for Recycling'. Gold Bull. 43 (3), 209–220. https://doi.org/10.1007/BF03214988.

Lennartsson, A., Engström, F., Samuelsson, C., Björkman, B., Pettersson, J., 2018. Large-Scale WEEE recycling integrated in an ore-based Cu-extraction system. Journal of Sustainable Metallurgy 4 (2), 222–232. https://doi.org/10.1007/s40831-018-0157-5.

Flores, G.R.A., Nikolic, S., Mackey, P.J., 2014. ISASMELT™ for the recycling of E-scrap and copper in the US case study example of a new compact recycling plant. JOM 66 (5), 823–832. https://doi.org/10.1007/s11837-014-0905-3.

Brusselaers, J., Mark, F.E., Tange, L., 2006. Using metal-rich WEEE plastics as feedstock/fuel substitute for an integrated metals smelter. PlasticsEurope, Brüssel, Belgium.

Khaliq, A., Rhamdhani, M.A., Brooks, G., Masood, S., 2014. Metal extraction processes for electronic waste and existing industrial routes: a review and Australian perspective. Resources 3 (1), 152–179. https://doi.org/10.3390/resources3010152.

Tesfaye, F., Lindberg, D., Hamuyuni, J., Taskinen, P., Hupa, L., 2017. Improving urban mining practices for optimal recovery of resources from e-waste. Miner. Eng. 111, 209–221. https://doi.org/10.1016/j.mineng.2017.06.018.

Anindya, A., Swinbourne, D., Reuter, M., & Matusewicz, R. (2009). Tin distribution during smelting of WEEE with copper scrap. In Proceedings of the European Metallurgical Conference EMC 2009, Innsbruck, Austria, 28 June-1 July 2009; GDMB Verlag GmbH: Clausthal-Zellerfeld, Germany, 2009; pp. 555-568.

Shuva M.A.H., Rhamdhani M.A., Brooks G.A., Masood S., Reuter M.A., & Firdaus M. (2017). Analysis for optimum conditions for recovery of valuable metals from E-waste through black copper smelting. In: 8th International Symposium on High-Temperature Metallurgical Processing (Ed. J-Y. Hwang et al.); TMS, Warrendale (PA), pp. 419-427. https://doi.org/10.1007/978-3-319-51340-9_41.

Chen, M., Avarmaa, K., Klemettinen, L., O'Brien, H., Sukhomlinov, D., Shi, J., Taskinen, P., Jokilaakso, A., 2020. Recovery of precious metals (Au, Ag, Pt, and Pd) from urban mining through copper smelting. Metallurgical and Materials Transactions B 51 (4), 1495–1508. https://doi.org/10.1007/s11663-020-01861-5.

Chen, M., Avarmaa, K., Klemettinen, L., O'Brien, H., Shi, J., Taskinen, P., Lindberg, D., Jokilaakso, A., 2021. Precious metal distributions between copper matte and slag at high P_{SO2} in WEEE reprocessing. Metallurgical and Materials Transactions B 52 (2), 871–882. https://doi.org/10.1007/s11663-021-02059-z.

Klemettinen, L., Avarmaa, K., O'Brien, H., Taskinen, P., Jokilaakso, A., 2019. Behavior of tin and antimony in secondary copper smelting process. Minerals 9 (1), 39. https://doi.org/10.3390/min9010039.

Klemettinen, L., Avarmaa, K., Taskinen, P., & Jokilaakso, A. (2018). Behavior of nickel as a trace element and time-dependent formation of spinels in WEEE smelting. In: Extraction 2018, Davis B. et al. (eds). The Minerals, Metals & Materials Series. Springer, Cham, 1073-1082. https://doi.org/10.1007/978-3-319-95022-8_86.

Dańczak, A., Klemettinen, L., Kurhila, M., Taskinen, P., Lindberg, D., Jokilaakso, A., 2020. Behavior of battery metals lithium, cobalt, manganese and lanthanum in black copper smelting. Batteries 6 (1), 16. https://doi.org/10.3390/batteries6010016.

Dańczak, A., Klemettinen, L., O'Brien, H., Taskinen, P., Lindberg, D., Jokilaakso, A., 2021. Slag chemistry and behavior of nickel and tin in black copper smelting with alumina and magnesia-containing slags. Journal of Sustainable Metallurgy 7 (1), 1–14. https://doi.org/10.1007/s40831-020-00318-y.

Avarmaa, K., Klemettinen, L., O'Brien, H., Taskinen, P., 2019. The behavior of tin in black copper smelting conditions with different iron-silicate based slags. In: In: *Proceedings of the European Metallurgical Conference EMC 2019*, pp. 23–26.

Avarmaa, K., & Taskinen, P. (2018b) The influence of aluminum on indium and tin behaviour during secondary copper smelting. In: Extraction 2018, Davis B. et al. (eds). The Minerals, Metals & Materials Series. Springer, Cham, 1061-1071. https://doi.org/10.1007/978-3-319-95022-8_85.

Avarmaa, K., Yliaho, S., & Taskinen, P. (2017) Indium, gallium and tin distributions between copper and slag in WEEE smelting conditions. In: Proceedings of the European Metallurgical Conference EMC 2017, vol 4, June 25-28, Leipzig, Germany. GDBM, Clausthal-Zellerfeld, 2017, 1485-1500.

Nagamori, M., Mackey, P.J., 1977. Distribution equilibria of Sn, Se and Te between FeO-Fe_2O_3-SiO_2-Al_2O_3-$CuO_{0.5}$ slag and metallic copper. Metall. Trans. B 8 (1), 39–46. https://doi.org/10.1007/BF02656349.

Ren, G., Xiao, S., Xia, L., Liao, C., Liu, Z., 2021. The distribution of cobalt between Co-Cu alloys and alumina-saturated MnO-SiO_2-Al_2O_3 slags. Metallurgical and Materials Transactions B 52 (1), 314–321. https://doi.org/10.1007/s11663-020-02015-3.

Derin, B., Yücel, O., 2002. The distribution of cobalt between Co-Cu alloys and Al_2O_3-FeO-Fe_2O_3-SiO_2 slags. Scand. J. Metall. 31 (1), 12–19. https://doi.org/10.1034/j.1600-0692.2002.310103.x.

Sukhomlinov, D., Avarmaa, K., Virtanen, O., Taskinen, P., Jokilaakso, A., 2020. Slag-copper equilibria of selected trace elements in black-copper smelting. Part II. Trace element distributions. Miner. Process. Extr. Metall. Rev. 41 (3), 171–177. https://doi.org/10.1080/08827508.2019.1634561.

Sukhomlinov, D., & Taskinen. P. (2017) Distribution of Ni, Co, Ag, Au, Pt, Pd between copper metals and silica saturated iron silicate slag. In: Proceedings of the European Metallurgical Conference EMC 2017, vol. 3, GDMB, Clausthal-Zellerfeld, 1029-1038.

Sukhomlinov, D., Klemettinen, L., Avarmaa, K., O'Brien, H., Taskinen, P., Jokilaakso, A., 2019a. Distribution of Ni Co, precious, and platinum group metals in copper making process. Metallurgical and Materials Transactions B 50 (4), 1752–1765. https://doi.org/10.1007/s11663-019-01576-2.

Ren, G., Xiao, S., Liao, C., Xia, L., Liu, Z., 2020. The activity coefficient of CoO in SiO_2 saturated MnO-SiO_2 slag at 1623 K. Metallurgical and Materials Transactions B 51 (4), 1339–1343. https://doi.org/10.1007/s11663-020-01837-5.

Kashima, M., Eguchi, M., Yazawa, A., 1978. Distribution of impurities between crude copper, white metal and silica-saturated slag. Transactions of the Japan Institute of Metals 19 (3), 152–158.

Van den Bulck, A., Turner, S., Guo, M., Malfliet, A., & Blanpain, B. (2018). The distribution of Sn between CaO-CuOx-FeOy-SiO2 slag and copper metal at 1300 °C. In: Extraction 2018, Davis B. et al. (eds). Springer, Cham, 1083-1092. https://doi.org/10.1007/978-3-319-95022-8_87.

Wang, S.S., Kurtis, A.J., Toguri, J.M., 1973. Distribution of copper-nickel and copper-cobalt between copper-nickel and copper-cobalt alloys and silica saturated fayalite slags. Can. Metall. Q. 12 (4), 383–390. https://doi.org/10.1179/cmq.1973.12.4.383.

Reddy, R.G., Healy, G.W., 1981. Distribution of cobalt between liquid copper and copper silicate slag at 1523 K. Metall. Trans. B 12 (3), 509–516.

Reddy, R.G., Healy, G.W., 1981. The Solubility of cobalt in Cu_2O-CoO-SiO_2 Slags in equilibrium with liquid Cu-Co alloys. Can. Metall. Q. 20 (2), 135–143. https://doi.org/10.1179/cmq.1981.20.2.135.

Reddy, R. G. (1980). Ph.D. Thesis: Distribution of cobalt between liquid copper-cobalt alloys and cuprous-silica slags, Dept. of Metallurgy and Metallurgical Engineering, University of Utah, Salt Lake City, Utah, December 1980.

Anindya, A., Swinbourne, D.R., Reuter, M.A., Matusewicz, R.W., 2013. Distribution of elements between copper and FeO_x-CaO-SiO_2 slags during pyrometallurgical processing of WEEE: Part 1-Tin. Mineral Processing and Extractive Metallurgy 122 (3), 165–173. https://doi.org/10.1179/1743285513Y.0000000043.

Kho, T.S., Swinbourne, D.R., Lehner, T., 2006. Cobalt distribution during copper matte smelting. Metallurgical and Materials Transactions B 37 (2), 209–214.

Gortais, J., Hodaj, F., Allibert, M., Welter, J.M., 1994. Equilibrium distribution of Fe, Ni, Sb, and Sn between liquid Cu and a CaO-rich slag. Metallurgical and Materials Transactions B 25 (5), 645–651.

Sukhomlinov, D., Klemettinen, L., O'Brien, H., Taskinen, P., Jokilaakso, A., 2019b. Behavior of Ga, In, Sn, and Te in copper matte smelting. Metallurgical and Materials Transactions B 50 (6), 2723–2732. https://doi.org/10.1007/s11663-019-01693-y.

Takeda, Y., Ishiwata, S., Yazawa, A., 1983. Distribution equilibria of minor elements between liquid copper and calcium ferrite slag. Transactions of the Japan Institute of Metals 24 (7), 518–528. https://doi.org/10.2320/matertrans1960.24.518.

Louey, R., Swinbourne, & D.R., Lehner, T. (1999). Silver and tin distribution between copper matte and fayalite slag. AusIMM Proceedings. The Australian Institute of Mining and Metallurgy, 31-36.

Tirronen, T., Sukhomlinov, D., O'Brien, H., Taskinen, P., Lundström, M., 2017. Distributions of lithium-ion and nickel-metal hydride battery elements in copper converting. J. Cleaner Prod. 168, 399–409. https://doi.org/10.1016/j.jclepro.2017.09.051.

Wang, S.S., Santander, N.H., Toguri, J.M., 1974. The solubility of nickel and cobalt in iron silicate slags. Metall. Trans. B 5 (1), 261.

Nagamori, M., & Mackey, P. J. (1978). Thermodynamics of copper matte converting: part II. Distribution of Au, Ag, Pb, Zn, Ni, Se, Te, Bi, Sb and As between copper, matte and slag in the Noranda process. Metallurgical Transactions B, 9(4), 567-579. https://doi.org/10.1007/BF03257205.

Teague, K.C., Swinbourne, D.R., Jahanshahi, S., 2001. A thermodynamic study on cobalt containing calcium ferrite and calcium iron silicate slags at 1573 K. Metallurgical and Materials Transactions B 32 (1), 47–54. https://doi.org/10.1007/s11663-001-0007-9.

Piskunen, P., Avarmaa, K., O'Brien, H., Klemettinen, L., Johto, H., Taskinen, P., 2018. Precious metal distributions in direct nickel matte smelting with low-Cu mattes. Metallurgical and Materials Transactions B 49 (1), 98–112. https://doi.org/10.1007/s11663-017-1115-5.

Hellstén, N., Klemettinen, L., Sukhomlinov, D., O'Brien, H., Taskinen, P., Jokilaakso, A., Salminen, J., 2019. Slag cleaning equilibria in iron silicate slag-copper systems. Journal of Sustainable Metallurgy 5 (4), 463–473. https://doi.org/10.1007/s40831-019-00237-7.

Nakajima, K., Takeda, O., Miki, T., Matsubae, K., Nagasaka, T., 2011. Thermodynamic analysis for the controllability of elements in the recycling process of metals. Environ. Sci. Technol. 45 (11), 4929–4936. https://doi.org/10.1021/es104231n.

Choi, N., Cho, W.D., 1997. Distribution behavior of cobalt, selenium, and tellurium between nickel-copper-iron matte and silica-saturated iron silicate slag. Metallurgical and Materials Transactions B 28 (3), 429–438. https://doi.org/10.1007/s11663-997-0109-0.

Xu, X., Hayes, P.C., Jak, E., 2013. Experimental study of phase equilibria in the "SnO"-CaO-SiO_2 system in equilibrium with tin metal. Int. J. Mater. Res. 104 (3), 235–243. https://doi.org/10.3139/146.110865.

Takeda, Y., Yazawa, A., Chit, P.P., Ujiie, H., 1990. Equilibria between liquid tin and FeO_x-CaO-SiO_2 Slag. Mater. Trans., JIM 31 (9), 793–801. https://doi.org/10.2320/matertrans1989.31.793.

Xu, X., Hayes, P.C., Jak, E., 2012. Phase equilibria in the "SnO"-SiO_2-"FeO" system in equilibrium with tin-iron alloy and the potential application for electronic scrap recycling. Int. J. Mater. Res. 103 (5), 529–536. https://doi.org/10.3139/146.110736.

Holland, Keiran, Sukhomlinov, Dmitry, Klemettinen, Lassi, Latostenmaa, Petri, O'Brien, Hugh, Jokilaakso, Ari, Taskinen, Pekka, 2019. Distribution of Co, Fe, Ni, and precious metals between blister copper and white metal. Mineral Processing and Extractive Metallurgy 1–11. https://doi.org/10.1080/25726641.2019.1643129.

Holland, K., Sukhomlinov, D., Naakka, V., Jokilaakso A., & Taskinen P. (2018) Behavior of Co, Ni and precious metals in copper converting process: experimental study. In: Energy Technology 2018, Sun Z. et al. (eds). The Minerals, Metals & Materials Series. Springer, Cham. https://doi.org/10.1007/978-3-319-72362-4_18.

Gisby, J., Taskinen, P., Pihlasalo, J., Li, Z., Tyrer, M., Pearce, J., Avarmaa, K., Björklund, P., Davies, H., Korpi, M., Martin, S., Pesonen, L., Robinson, J., 2017. MTDATA and the prediction of phase equilibria in oxide systems: 30 years of industrial collaboration. Metallurgical and Materials Transactions B 48 (1), 91–98. https://doi.org/10.1007/s11663-016-0811-x.

Davies, R.H., Dinsdale, A.T., Gisby, J.A., Robinson, J.A.J., Martin, A.M., 2002. MTDATA-thermodynamic and phase equilibrium software from the national physical laboratory. Calphad 26 (2), 229–271. https://doi.org/10.1016/S0364-5916(02)00036-6.

Roine, A. (2017) HSC Chemistry for Windows, v. 9.4.1 (Pori, Finland: Outotec Research, 2017). https://www.hsc-chemistry.com/news&tiedoteid=31.

Avarmaa, Katri, Klemettinen, Lassi, O'Brien, Hugh, Taskinen, Pekka, 2019. Urban mining of precious metals via oxidizing copper smelting. Miner. Eng. 133, 95–102. https://doi.org/10.1016/j.mineng.2019.01.006.

Avarmaa, K., O'Brien, H., Klemettinen, L., Taskinen, P., 2020. Precious metal recoveries in secondary copper smelting with high-alumina slags. J. Mater. Cycles Waste Manage. 22 (3), 642–655. https://doi.org/10.1007/s10163-019-00955-w.

Klemettinen, L., Avarmaa, K., Taskinen, P., 2017. Slag chemistry of high-alumina iron silicate slags at 1300 °C in WEEE smelting. Journal of Sustainable Metallurgy 3 (4), 772–781. https://doi.org/10.1007/s40831-017-0141-5.

Avarmaa K., O'Brien H., & Taskinen P. (2016) Equilibria of gold and silver between molten copper and FeOx-SiO2-Al2O3 Slag in WEEE smelting at 1300 °C. In: Reddy R. G., Chaubal P., Pistorius P.C., Pal U. (eds) Advances in Molten Slags, Fluxes, and Salts: Proceedings of the 10th International Conference on Molten Slags, Fluxes and Salts 2016. Springer, Cham. https://doi.org/10.1007/978-3-319-48769-4_20.

Pouchou, J.L. & Pichoir, F. (1986). Basic expression of "PAP" computation for quantitative EPMA. In: Brown, J.D. & Packwood, R.H. (eds.) 11th international Congress on X-ray Optics and Microanalysis (ICXOM), 249-253.

Van Achterbergh, E., R. C.G., S.E. Jackson, & G. W.L. (2001). Data reduction software for LA-ICP-MS: appendix. P.J. Sylvester (Ed.), Laser Ablation-ICP-Mass Spectrometry in the Earth Sciences: Principles and Applications, Mineralog. Assoc. Canada (MAC) Short Course Series, Ottawa, Ontario, Canada, vol. 29, 239-243.

Hidayat, T., Chen, J., Hayes, P.C., Jak, E., 2021. Distributions of As, Pb, Sn and Zn as minor elements between iron silicate slag and copper in equilibrium with tridymite in the Cu-Fe-O-Si system. Int. J. Mater. Res. 112 (3), 178–188. https://doi.org/10.1515/ijmr-2020-7857.

Hidayat, T., Chen, J., Hayes, P.C., Jak, E., 2019. Distributions of Ag, Bi, and Sb as minor elements between iron-silicate slag and copper in equilibrium with tridymite in the Cu-Fe-O-Si system at $T = 1250$ °C and 1300 °C (1523 K and 1573 K). Metallurgical and Materials Transactions B 50 (1), 229–241. https://doi.org/10.1007/s11663-018-1448-8.

Sineva, S., Shishin, D., Starykh, R., Hayes, P.C., Jak, E., 2021. Equilibrium distributions of Pb, Bi, and Ag between fayalite slag and copper-rich metal, calcium ferrite slag and copper-rich metal. In: thermodynamic assessment and experimental study at 1250 °C. *Journal of Sustainable Metallurgy*. https://doi.org/10.1007/s40831-021-00360-4.

Park, J. H., & Min, D. J. (1999). Quantitative analysis of the relative basicity of CaO and BaO by silver solubility in slags. Metallurgical and Materials Transactions B, 30(4), 689-694.

Kaur, R.R., Swinbourne, D.R., Nexhip, C., 2009. Nickel, lead and antimony distributions between ferrous calcium silicate slag and copper at 1300 C. Mineral Processing and Extractive Metallurgy 118 (2), 65–72. https://doi.org/10.1179/174328509X383890.

Reddy, R.G., Acholonu, C.C., 1984. Distribution of nickel between copper-nickel and alumina saturated iron silicate slags. Metall. Trans. B 15 (1), 33–37.

Starykh, Roman, Shevchenko, Maksym, Shishin, Denis, Jak, Evgueni, 2021. Experimental study and thermodynamic modeling of the Cu-Sn-Si-O system and sub-systems. Calphad 74, 102312. https://doi.org/10.1016/j.calphad.2021.102312.

Avarmaa, K., Yliaho, S., Taskinen, P., 2018a. Recoveries of rare elements Ga, Ge, In and Sn from waste electric and electronic equipment through secondary copper smelting. Waste Manage. 71, 400–410. https://doi.org/10.1016/j.wasman.2017.09.037.

Berry, F.J., Skinner, S.J., Helgason, O., Bilsborrow, R., Marco, J.F., 1998. Location of tin and charge balance in materials of composition $Fe_{3\text{-}x}Sn_xO_4$ ($x<0.3$). Polyhedron 17 (1), 149–152. https://doi.org/10.1016/S0277-5387(97)00212-X.

Lu, F.H., Dieckmann, R., 1995. Point defects in oxide spinel solid solutions of the type (Co, Fe, $M_{n)3\text{-}\sigma}$O4 at 1200 °C. J. Phys. Chem. Solids 56 (5), 725–733. https://doi.org/10.1016/0022-3697(94)00187-1.

Salazar-Tamayo, H., García, K.E., Barrero, C.A., 2019. New method to calculate Mössbauer recoilless f-factors in $NiFe_2O_4$. Magnetic, morphological and structural properties. J. Magn. Magn. Mater. 471, 242–249. https://doi.org/10.1016/j.jmmm.2018.09.066.